Applied Catalysis A: General 431–432 (2012) 95–103

Contents lists available at SciVerse ScienceDirect

Applied Catalysis A: General

journal homepage: www.elsevier.com/locate/apcata

Organometal-bridged PMOs as efficiency and reusable bifunctional catalysts in one-pot cascade reactions

Jianlin Huang[a], Fang Zhang[a], Hexing Li[a,b,*]

[a] Department of Chemistry and The Education Ministry Key Lab of Resource Chemistry, Shanghai Normal University, Shanghai 200234, PR China
[b] Department of Chemistry, Shanghai University of Electric Power, Shanghai 200090, PR China

ARTICLE INFO

Article history:
Received 21 February 2012
Received in revised form 5 April 2012
Accepted 15 April 2012
Available online 21 April 2012

Keywords:
Bifunction catalysts
Periodic mesoporous organosilicas (PMOs)
Organometal-bridged PMO
Surfactant directed co-condensation
One-pot cascade reactions
Asymmetric reaction

ABSTRACT

Two bifunctional catalysts with two kinds of organometals incorporated into the periodic mesoporous organosilica (PMO) supports, denoted as Rh/Pd@PMO(Ph) catalyst and Fe/Cp*Rh@PMO(Et) chiral catalyst, were synthesized by surfactant directed co-condensation between phenyl (Ph)- or ethyl (Et)-bridged and organometal-bridged silanes. Two bifunctional catalysts exhibited high activities and selectivities and even high ee values in one-pot two-step cascade reactions comprised Rh(I)-catalyzed methylenation and Pd(II)-catalyzed Heck reaction, or Fe(III)-catalyzed hydrolysis and Cp*Rh-catalyzed asymmetric hydrogenation. The promoting effects from the ordered mesoporous structure, the coordination model, and the synergic effect between two kinds of active sites were discussed based on the detailed characterizations. Their catalytic efficiencies were comparable with the corresponding homogeneous catalysts and could be easily recycled and used repetitively, which could greatly reduce the cost and diminish the environmental pollutions from heavy metal ions.

1. Introduction

Since the discovery of M41S, organic–inorganic composite materials with ordered and open porous structure have been widely studied owing to their potential applications in catalysis, adsorption, separation, etc., most studies have devoted to designing mesoporous organic–inorganic hybrid silicas [1–4]. Organic groups including methyl, ethyl, phenyl, biphenyl and amine have been successfully incorporated into ordered mesoporous silicas through either grafting the organotrialkoxysilanes $RSi(OR)_3$ or the direct co-assembly of organo-bridged silanes, resulting in the organic groups terminally bonded to the pore surface [5,6] or the periodic mesoporous organosilica (PMO) with organic groups as the integral part of the pore walls [7–11]. Learning from those achievements, we developed a facile approach to design immobilized homogeneous catalysts with combined advantages from both the homogeneous catalysts (e.g., high activity and selectivity) [12,13] and the heterogeneous catalysts (e.g., easy recycle and reuse) by either grafting organometals onto pore surface [14,15] or incorporating organometals into silica walls of the mesoporous channels [16,17]. The chiral organometal catalysts were also successfully grafted onto mesoporous silica supports, which exhibited high activities and even ee values in various asymmetric reactions [18]. More recently, we also synthesized a new class of heterogenized homogeneous catalysts by immobilizing organometals onto the phenol–formaldehyde resin with ordered mesoporous structure [19].

As an expressly practical science, synthetic organic chemistry counts as one of its primary aims at the invention of efficient, rapid and economical strategies to gain valuable chemical substances [20,21]. One-pot cascade or tandem organic reactions have received great attentions since they could simplify the operation procedure in intermediate product purification or detections and also diminish the environmental pollution [22,23]. The key stone to realize the one-pot cascade or tandem organic reactions is the design of powerful multiple-functional catalysts, which allow to alleviating dependency on strictly reduplicative processes [24–26]. To date, most cascade and tandem organic reactions are conducted in homogeneous catalyst systems [27], which usually display inherent disadvantages in difficult recycle, leading to the high cost and even the environmental pollutions from heavy metal ions. Meanwhile, the cross-interference between different kinds of active sites also frequently occurs in homogeneous catalytic systems [28]. Heterogeneous catalysts are easily recycled and used repetitively, however, they usually display poor activities and selectivities due to the enhanced steric hindrance and the changed chemical microenvironment of active sites [29,30]. Our strategy for the design of heterogeneous multiple functional catalysts focuses on the

* Corresponding author at: Department of Chemistry and The Education Ministry Key Lab of Resource Chemistry, Shanghai Normal University, Shanghai 200234, PR China. Tel.: +86 21 64322642; fax: +86 21 64322272.
E-mail address: hexing-li@shnu.edu.cn (H. Li).

0926-860X/$ – see front matter © 2012 Elsevier B.V. All rights reserved.
http://dx.doi.org/10.1016/j.apcata.2012.04.021

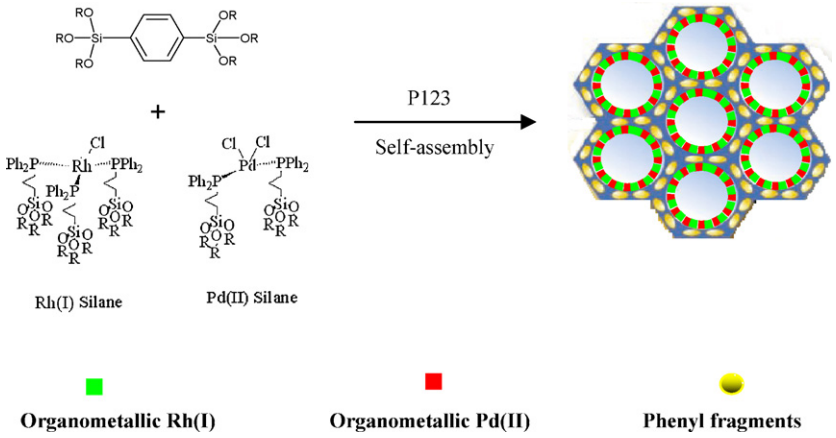

Scheme 1. Illustration of preparing Rh/Pd@PMO(Ph) bifunctional catalyst.

controlled assembly of different active sites onto the silica supports with ordered mesoporous structure, which allows to adjust the distance between different active sites with the aim to promote their synergistic effect and inhibit their cross-interference. Meanwhile, the ordered mesoporous channels and the modification of silica walls with organic groups including phenyl and ethyl could facilitate the diffusion of reactant molecules [14]. Herein, we reported two bifuctionalized catalysts with two kinds of organometal catalysts homogeneously incorporated into silica walls of the PMO supports, which were used in one-pot cascade reactions comprised Rh(I)-catalyzed methylenation and Pd(II)-catalyzed Heck reaction, or Fe(III)-catalyzed hydrolysis and Cp*Rh-catalyzed asymmetric hydrogenation. As expected, these catalysts exhibited high activities and selectivities, and even high ee values, almost comparable with the corresponding homogeneous catalyst systems. More importantly, they could be easily recycled and used repetitively.

2. Experimental

2.1. Catalyst preparation

Firstly, $RhCl[PPh_2(CH_2)_2Si(EtO)_3]_3$ and $PdCl_2[PPh_2(CH_2)_2Si(EtO)_3]_2$ organometal silanes were synthesized by the cross coordination as reported previously [17]. Then, the Rh/Pd@PMO(Ph) bifunctional catalyst was synthesized by surfactant directed co-condensation of bis(triethoxysilyl)benzene (BTESB), Rh(I) and Pd(II) organometal silanes (see Scheme 1), where PMO(Ph) refers to the phenyl (Ph)-bridged periodic mesoporous organoslica (PMO). Briefly, a certain amount of BTESB was introduced into 40 mL HCl (0.20 M) aqueous solution containing 1.0 g P123 ($EO_{20}PO_{70}EO_{20}$) and 3.0 g KCl. After the BTESB was prehydrolyzed for 45 min under stirring at 40 °C, the Rh(I) and Pd(II) organometal silanes dissolved in THF solution was added dropwise into the above solution, followed by rapidly stirring for 24 h at 40 °C. After being aged at 100 °C for 24 h, the resulted brown precipitate was filtrated and vacuum dried at 80 °C overnight. Finally, the surfactant and other organic substances were extracted and washed away by refluxing in HCl/ethanol solution at 80 °C for 24 h. The initial molar ratio in the mother solution was fixed at Si:P123:HCl:H_2O:KCl = 1:0.031:1.43:1.68:393:7.14, where Si refers to the total silica source in BTESB, Rh(I) and Pd(II) organometal silanes. The Rh(I) and Pd(II) loadings in the catalyst were adjusted by changing the contents of Rh(I) and Pd(II) organometal-bridged silanes in the initial mixture, which were designed as Rh/Pd@PMO(Ph)-2.5, Rh/Pd@PMO(Ph)-5.0, Rh/Pd@PMO(Ph)-7.5, Rh/Pd@PMO(Ph)-10 and Rh/Pd@PMO(Ph)-15, corresponding to 2.5%, 5.0%, 7.5%, 10%, and 15% molar ratios of total Rh(I) and Pd(II) silanes in the initial mixture. Meanwhile, the monofunctional catalysts, denoted as Rh@PMO(Ph) and Pd@PMO(Ph) were prepared in the similar way by using the individual Rh(I) or Pd(II) silane instead of the mixed Rh(I) and Pd(II) silanes.

The Cp*Rh@PMO(Et) chiral catalyst was prepared by the following procedure. Firstly, 0.75 g 2-(4-chlorosulfonylphenyl) ethyltrimethoxysilane (CSPES) was added dropwise into 30 mL CH_2Cl_2 solution containing 0.64 g (1*R*, 2*R*)-DPEN and 0.60 mL $(Et)_3N$ (triethylamine) at 0 °C, followed by stirring at 27 °C for 3 h. After evaporation of solvents under vacuum, the residue was allowed to pass through a short silica gel column by using an eluent containing Et_3N, CH_3OH, CH_2Cl_2 with the molar ratio of 1:10:100. The as-received silane containing a chiral ligand was denoted as TsDPEN. Subsequently, 1.0 g TsDPEN was dissolved in CH_3OH solution and mixed with 80 mL 0.50 mol/L HCl solution containing 2.6 g P123 (EO_{20}–PO_{70}–EO_{20}, M_{avg} = 5800), 7.0 g NaCl and 4.2 mL $(EtO)_3SiCH_2CH_2(EtO)_3$. The mixture was stirred at 40 °C for 24 h, followed by hydrothermal treatment at 80 °C for another 24 h. The solid product was filtrated and extracted in 500 mL EtOH solution at 80 °C for 24 h to remove surfactant template and other organic residues, followed by drying under vacuum. The as-received sample was denoted as TsDPEN-PMO(Et). Then, 0.20 g TsDPEN-PMO(Et) was dissolved in 6.0 mL CH_2Cl_2, followed by adding 0.040 g $(Cp^*RhCl_2)_2$ and stirring at 25 °C for 20 h. The solid product was filtrated, washed with CH_2Cl_2 for 3 times, vacuum dried at 60 °C for 6 h, followed by Soxlet-extraction with toluene to remove all impurities including the physisorbed $(Cp^*RhCl_2)_2$ species and then drying overnight under vacuum at room temperature, leading to the Cp*Rh@PMO(Et) chiral catalyst, where Cp* refers to pentamethylcyclopentadiene.

For comparison, the bifunctional catalyst with Pd(II) and Rh(I) organometals terminally bonded to the pore surface of the PMO(Ph) support was also synthesized by grafting method and denoted as Rh/Pd@PPh_2-PMO(Ph). Firstly, 1.0 g P123 and 3.0 g KCl are dissolved in 40 mL 0.067 M HCl aqueous solution and stirred for 2 h, followed by mixing with 1.0 g BTESB and 0.21 g $PPh_2CH_2CH_2Si(OEt)_3$ (DPPTS). The mixture was stirred for 24 h at 40 °C and kept at 100 °C for another 24 h. The solid product was extracted in 0.50 M HCl/ethanol solution at 80 °C for 24 h, leading to the pure PPh_2-PMO(Ph). Then, 1.0 g PPh_2-PMO(Ph) was added into 30 mL toluene solution containing 63 mg $RhCl(PPh_3)_3$ and 48 mg $PdCl_2(PPh_3)_2$, followed by stirring for 24 h at 30 °C under argon atmosphere. After Soxlet-extraction in toluene solvent to remove unreacted $RhCl(PPh_3)_3$ and $PdCl_2(PPh_3)_2$, the Rh/Pd@PPh_2-PMO(Ph) was vacuum dried at 80 °C for 24 h and kept under vacuum until the time of use. The $FeCl_3$ was commercially available and used without further purification.

2.2. Catalyst characterization

Fourier transform infrared (FTIR) spectra were collected with a Nicolet Magna 550 spectrometer by using the KBr method. Solid-state NMR spectra were recorded on a Bruker AV-400 spectrometer. The X-ray powder diffraction (XRD) patterns were obtained from a Rigaku D/Max-RB diffractometer with CuKα radiation. Transmission electron microscopy (TEM) images were observed on a JEOL JEM2010 electron microscope at an acceleration voltage of 200 kV. N_2 adsorption–desorption isotherms were measured at −196 °C on a Quantachrome NOVA 4000e analyzer, from which the specific surface area (S_{BET}), the pore volume (V_P) and the average pore diameter (D_P) were calculated by applying multiple-point Brunauer–Emmett–Teller (BET) and Barrett–Joyner–Halenda (BJH) models on adsorption branches. Thermogravimetric analysis and differential thermal analysis (TG/DTA) were conducted on a DT-60. The surface electronic states were analyzed by X-ray photoelectron spectroscopy (XPS, Perkin-Elmer PHI 5000C ESCA). All the binding energy values are calibrated by using C_{1S} = 284.8 eV as a reference. The real metal loadings in the catalysts were determined by inductively coupled plasma optical emission spectrometer (ICP, Varian VISTA-MPX).

2.3. Activity test

The one-pot cascade reaction comprising sequential Rh(I)-catalyzed cinnamaldehyde methylenation and Pd(II)-catalyzed Heck reaction (Eq. (1)) was employed to examine the performance of the Rh/Pd@PMO(Ph) bifunctional catalyst. In a typical run of reactions, a Rh/Pd@PMO(Ph)-10 catalyst containing 0.13 mmol Rh and 0.040 mmol Pd was added into the mixture containing 1.0 mmol cinnamaldehyde, 1.4 mmol trimethylsilyldiazomethane, 1.1 mmol *i*PrOH, 1.1 mmol PPh_3, 1.0 mmol iodobenzene and 5.0 mL THF, followed by refluxing at 60 °C under stirring for 24 h. Then, the mixture was extracted by ether and dried by $MgSO_4$. The reaction products were identified by GC–MS and quantitative analyzed on a GC-17A gas chromatograph (Shimadzu) equipped with a JWDB-5 column containing 95% dimethyl 1-(5%)-diphenylpolysiloxane and a FID detector. The column temperature was programmed from 80 to 250 °C at a speed of 10 °C/min. N_2 flow was used as carrier gas and *n*-decane was used as an internal standard. The conversion and selectivity were calculated based on the product analysis. Meanwhile, the one-pot cascade reaction comprised sequential Fe(III)-catalyzed phenylacetylene hydrolysis and Cp*Rh-catalyzed asymmetric hydrogenation (Eq. (2)). Reaction conditions: a Cp*Rh@PMO(Et) catalyst containing 0.010 mmol Cp*Rh, 1.0 mmol $FeCl_3$, 1.0 mmol phenylacetylene, 1.5 mmol HCOONa (pH = 8.0–10), 4.0 mL H_2O, reaction temperature = 40 °C, reaction time = 24 h. Products were extracted by ethyl acetate, followed by quantitative analysis with a chiral column (30 m × 0.25 mm (i.d.), 0.25 μm film).

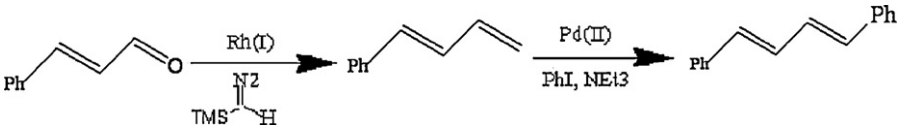

(1)

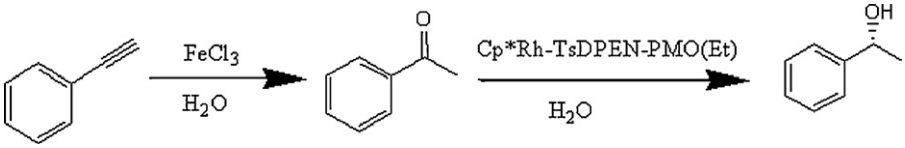

(2)

The reproducibility of all results was checked by repeating the results at least three times and was found to be within acceptable limits (±5%). In order to determine the catalyst durability, the Rh/Pd@PMO(Ph)-10 catalyst was allowed to settle down after each run of reactions and the clear supernatant liquid was decanted slowly. The residual solid catalyst was re-used with fresh charge of solvent and reactant for subsequent recycle runs under the same reaction conditions. The content of Rh or Pd species leached off from the Rh/Pd@PMO(Ph)-10 heterogeneous catalyst in each run was determined by ICP analysis.

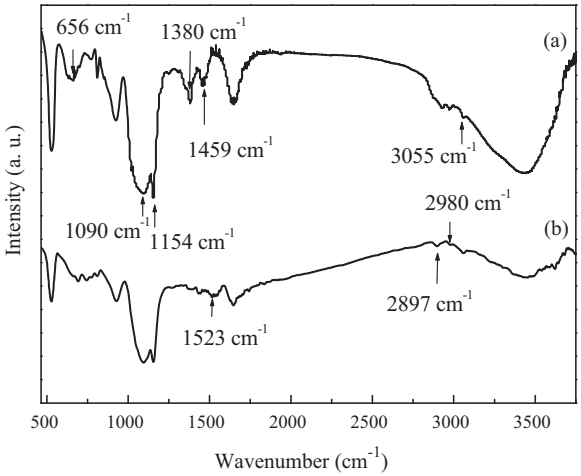

Fig. 1. FTIR spectra of (a) PMO(Ph) and (b) Rh/Pd@PMO(Ph)-10.

3. Results and discussion

3.1. Structural characteristics

The FTIR spectra in Fig. 1 revealed that both the PMO(Ph) and the Rh/Pd@PMO(Ph)-10 displayed three peaks at around 656, 1459 and 3055 cm^{-1} indicative of δ(C—H), ν(C—C) and ν(C—H) in benzene ring [31]. Two peaks at 1090 and 1154 cm^{-1} were designated to the ν(Si—O) and ν(Si—C) vibrations, respectively [32]. In comparison with the pure PMO(Ph), the Rh/Pd@PMO(Ph)-10 exhibited two additional peaks at 2897 and 2980 cm^{-1} indicative of the ν(C—H) vibrations from the CH_2—CH_2 group and another peak around 1523 cm^{-1} corresponding to the ν(P—C) vibration [33], showing the successful co-assemblies of the organometal silane complexes and BTESB. This could also account for the abrupt intensity decrease of the peak at 3500 cm^{-1}, taking into account of the substitution of OH-groups by the organometal complexes. Fig. 2 shows the solid NMR spectra of Rh/Pd@PMO(Ph)-10. The ^{29}Si MAS spectrum displayed three peaks down-field corresponding to T^1 (δ = −63 ppm), T^2 (δ = −73 ppm) and T^3 (δ = −81 ppm), where $T_m = RSi(OSi)_m–(OH)_{3-m}$, m = 1–3. No Q_n peaks were observed, where $Q_n = Si(OSi)_n–(OH)_{4-n}$, n = 2–4, indicating that all the Si species were covalently bonded with carbon atoms, i.e., all of the Si—C bonds remained intact in Rh/Pd@PMO(Ph)-10 [34]. Evidently,

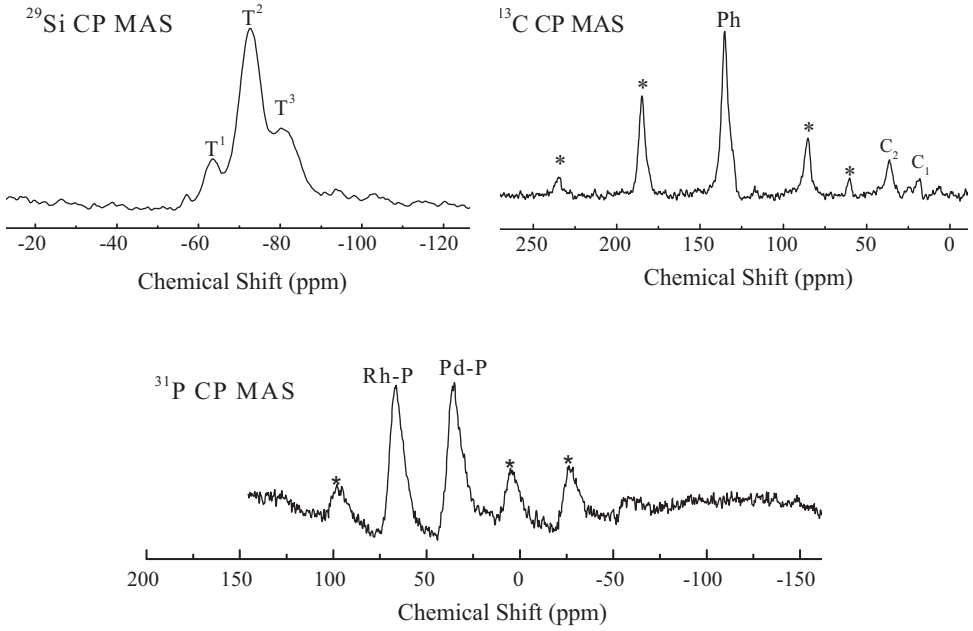

Fig. 2. Solid NMR spectra of the Rh/Pd@PMO(Ph)-10 catalyst.

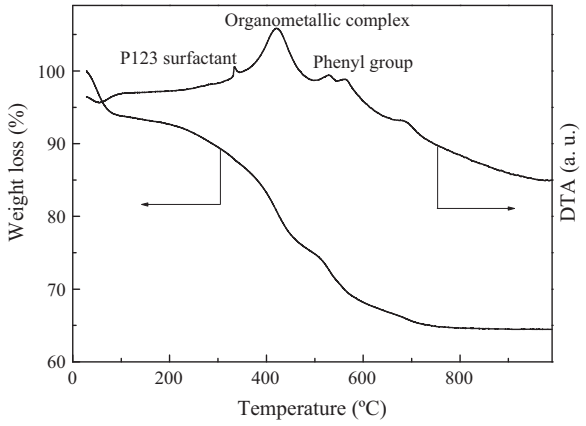

Fig. 3. TG/DTA curves the Rh/Pd@PMO(Ph)-10 catalyst.

the stronger T^2 peak than either the T^1 or the T^3 peaks suggested a high degree of cross-linking framework [35]. Meanwhile, the ^{13}C CP MAS clearly displayed two peaks at around 10 and 33 ppm, corresponding to two C atoms in the $-CH_2-CH_2-$ connecting with the PPh_2-group and one peak around 138 ppm indicative of the C atoms in the benzene ring in the sample [36]. Furthermore, the ^{31}P CP MAS exhibited two evident signals at 35 and 67 ppm, corresponding to the Pd—P and Rh—P coordination bonds [37], respectively. All of these results demonstrated that the organometal complexes and the Ph-groups successfully incorporated into the PMO network without significant decomposition.

The TG/DTA curves (Fig. 3) revealed that the Rh/Pd@PMO(Ph)-10 displayed about 7% weight loss below 100 °C, corresponding to the removal of physisorbed water and other solvents. A small exothermic peak with 6% weight loss was observed around 300 °C, which could be attributed to the oxidation of P123 [38], implying the presence of trace surfactant template after extraction in HCl/ethanol solution. Meanwhile, an extensive exothermic peak with about 12% weight loss appeared around 420 °C, corresponding to the decomposition of organometal complexes [39]. In addition, other exothermo peaks ranging from 500 to 650 °C with weight loss around 10% could be attributed to the oxidation of the phenyl groups incorporated into the silica walls [35].

As shown in Fig. 4, the XPS spectra revealed that the Rh and the Pd species in the Rh/Pd@PMO(Ph)-10 catalyst were present in pure +1 and +2 oxidation states, respectively, corresponding to the binding energies of 307.5 and 343.7 eV in $Rh_{3d5/2}$ and $Pd_{3d5/2}$ levels [40]. The binding energy of either the Rh(I) and the Pd(II) in Rh/Pd@PMO(Ph)-10 shifted negatively in comparison with the corresponding Rh(I) and Pd(II) in $RhCl(PPh_3)_3$ and $PdCl_2(PPh_3)_2$, suggesting that either the Rh(I) or the Pd(II) accepted more electrons from the $PPh_2CH_2CH_2$-ligand than that from the PPh_3-ligand. This could be attributed to the weaker electron-donation ability of the PPh_3-ligand than the $PPh_2—CH_2—CH_2$-ligand due to dilution effect of electrons in the conjugated π–π system between one P atom with three Ph groups, leading to the lower electron density on the P atom [41]. Other Rh/Pd@PMO(Ph) samples displayed almost the same XPS spectra as the Rh/Pd@PMO(Ph)-10. Meanwhile, the Rh(I) and Pd(II) organometal silanes displayed the similar XPS spectra to the Rh/Pd@PMO(Ph) in the Rh_{3d} and Pd_{3d} levels, respectively, suggesting that those organometal silanes integrally incorporated into the PMO(Ph) network without significant change of the chemical microenvironments.

Fig. 5 demonstrated that all the Rh/Pd@PMO(Ph) catalysts displayed type-IV nitrogen adsorption–desorption isotherms with H1-type hysteresis loop indicative of the mesoporous structure [42] with the narrow pore size distribution (see the attached pore size distribution curves). An abrupt step in the relative pressure at $p/p_0 = 0.45$ was observed due to the capillary condensation of nitrogen in mesopores. The increase of the organometal loading had no significant influence on the shape of H1-type hysteresis loop owing to the preservation of the mesoporous structure. The XRD patterns revealed that all the Rh/Pd@PMO(Ph) catalysts exhibited a well resolved peak at $2\theta = 0.80°$ characteristic of the (1 0 0) diffraction, suggesting the formation of ordered 2-dimensional p6mm hexagonal mesoporous structure [43]. The $d_{1\,0\,0}$ reflection gradually decreased with the increase of the organometal loading, indicating the enhanced wall thickness. Meanwhile, the peak intensity also decreased gradually with the increase of the organometal loading,

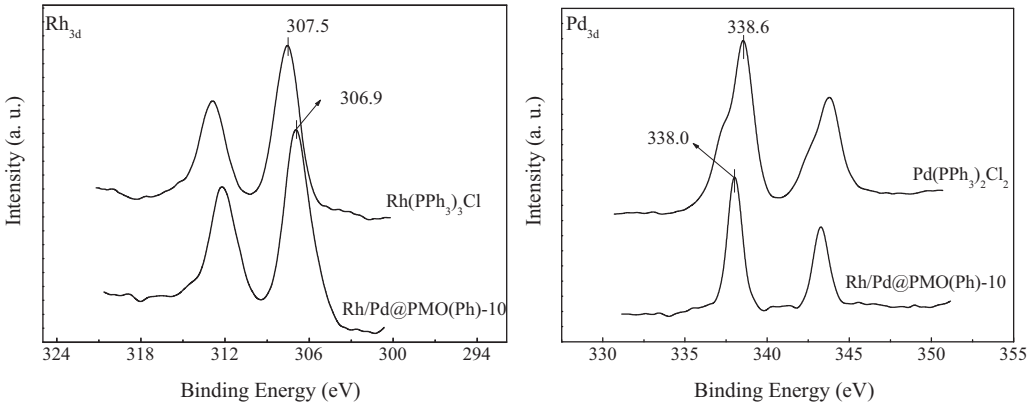

Fig. 4. XPS spectra of Rh/Pd@PMO(Ph)-10, $Rh(PPh_3)_3Cl$ and $Pd(PPh_3)_2Cl_2$.

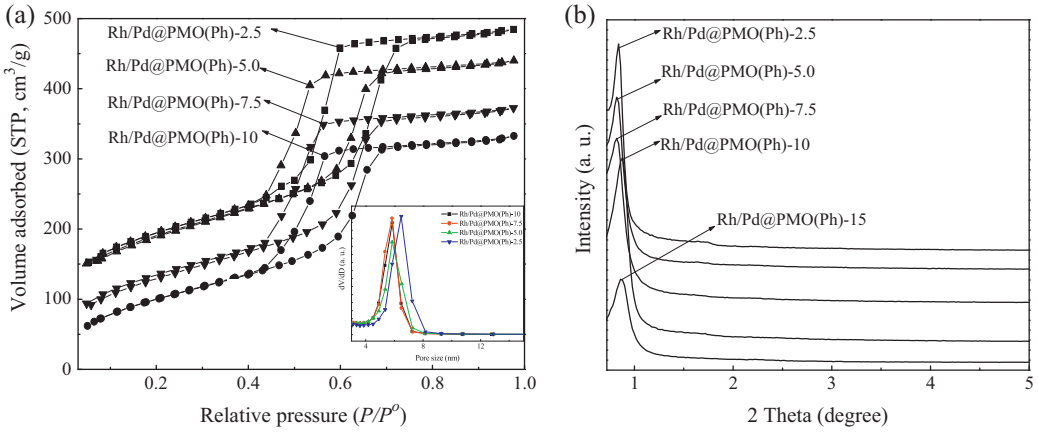

Fig. 5. (a) N_2 adsorption–desorption isotherms (the attached pore size distribution curves) and (b) low-angle XRD patterns of different Rh/Pd@PMO(Ph) catalysts.

implying the decrease in the ordering degree of mesoporous structure, possibly due to the disturbance of the surfactant self-assembly into micelles [44]. The Rh/Pd@PMO(Ph)-15 exhibited an abrupt decrease in the peak intensity, indicating the partial damage of ordered mesoporous structure. As shown in Fig. 6, the TEM images further confirmed the ordered 2-dimensional hexagonal mesopore channels in all the Rh/Pd@PMO(Ph) catalysts and the visible damage of the ordered mesopore channels in the Rh/Pd@PMO(Ph)-15. Similarly, the nitrogen adsorption–desorption isotherms, low-angle XRD patterns and TEM images (Fig. 7(a)) also demonstrated that the Cp*Rh@PMO(Et) displayed ordered mesoporous structure.

Some structural parameters are summarized in Table 1. In comparison with the Rh/Pd@PPh_2-PMO(Ph)-10 synthesized by grafting method, the Rh/Pd@PMO(Ph)-10 prepared via co-condensation exhibited much higher specific surface area (S_{BET}), pore diameter (D_P) and pore volume (V_P), which could mainly attributed to the different locations of the organometals taking into account that those two catalysts displayed almost the same Rh(I) and Pd(II) loadings. Unlike the Rh/Pd@PMO(Ph)-10 in which the Rh(I) and Pd(II) organometals were incorporated into the silica walls of the PMO(Ph) support, the Rh/Pd@PPh_2-PMO(Ph)-10 contained the Rh(I) and Pd(II) organometals mainly bonded terminally onto the pore surface, which inevitably blocked the pore channels [45], although it also displayed ordered mesoporous structure (see Fig. 7(b)). For the Rh/Pd@PMO(Ph) series catalysts, only slight decrease in S_{BET}, D_P and V_P was observed with the increase of Rh(I) and Pd(II) loading, which could mainly attributed to the presence of organometals in silica walls, leading to the enhanced wall thickness (see the aforementioned XRD patterns). The Rh/Pd@PMO(Ph)-15 exhibited abrupt decrease in S_{BET}, D_P and V_P, obviously due to the damage of ordered mesoporous structure at very high content of Rh(I) and Pd(II) organometals, as discussed above.

A key consideration of the immobilized catalyst was that the active sites should be exposed and chemically accessible with the reactant molecules during catalytic reactions [10]. To determine the location of organometal species, we used the Rh@PMO(Ph) as a model catalyst to do the following experiments. Firstly, the Rh@PMO(Ph) catalyst was allowed to react with $KMnO_4$ in aqueous solution for enough time. The unreacted $KMnO_4$ was titrated quantitatively by $Na_2C_2O_4$. The Rh(I) content determined by $KMnO_4$ oxidation could be considered as the Rh(I) species accessible for catalytic reactions. Meanwhile, the total Rh(I) species were determined by ICP analysis. The experimental results revealed that the molar ratio between Rh(I) species determined by $KMnO_4$ oxidation and the total Rh(I) species determined by ICP analysis was around 94%, suggesting that most of the Rh(I) active sites in the Rh@PMO(Ph) catalyst were accessible for catalytic reactions. Thus, we concluded that, although the organometals were incorporated into the silica walls of the PMO supports in the as-prepared catalysts, the metal active sites were mainly located on the pore surface and were chemically accessible for the catalytic reactions.

3.2. Catalytic performances

The performances of two bifunctional catalysts were evaluated in different one-pot cascade reactions comprised two steps of sequential reactions. Firstly, we examined the catalytic efficiencies of the Rh/Pd@PMO(Ph) in an one-pot

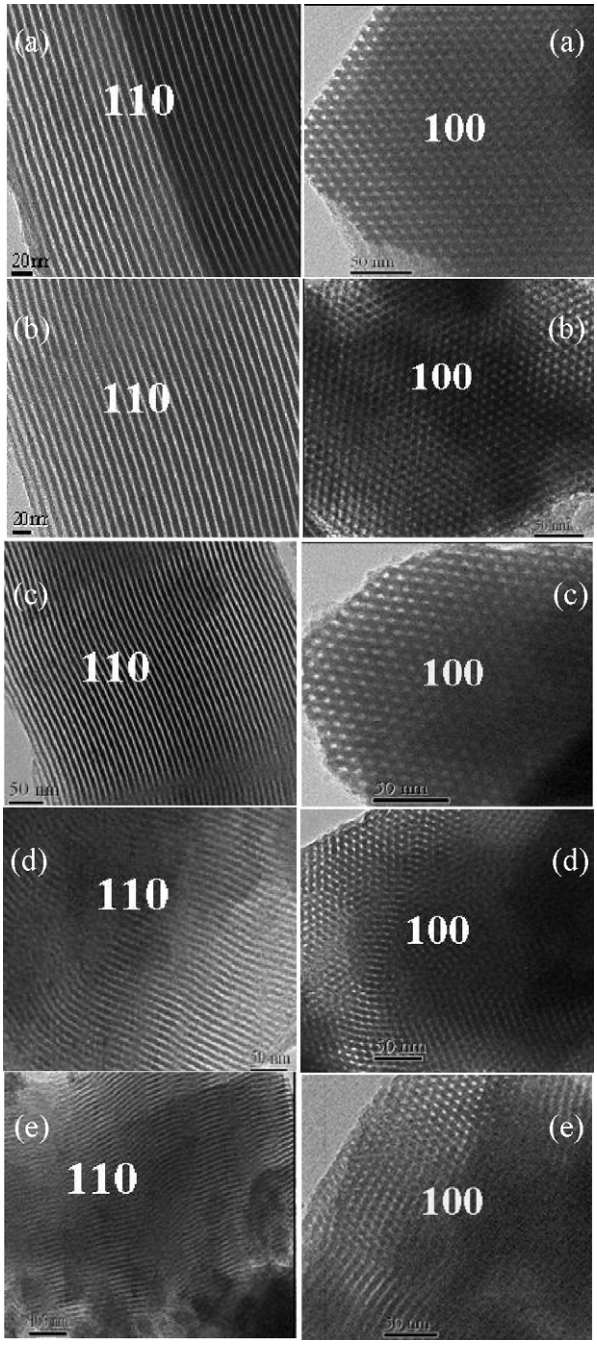

Fig. 6. TEM images of (a) Rh/Pd@PMO(Ph)-2.5, (b) Rh/Pd@PMO(Ph)-5.0, (c) Rh/Pd@PMO(Ph)-7.5, (d) Rh/Pd@PMO(Ph)-10, and (e) Rh/Pd@PMO(Ph)-15 catalysts along [1 1 0] and [1 0 0] directions, respectively.

cascade reaction containing the subsequent Rh(I)-catalyzed cinnamaldehyde methylenation and Pd(II)-catalyzed Heck reaction (see Eq. (1)). The conversion was calculated based on cinnamaldehyde since other reactants were excess. Meanwhile, the selectivity was determined based on transformation of 1-phenyl-1,3-butadiene to 1,4-diphenyl-1,3-butadiene. Firstly, we examined the roles played by individual Rh@PMO(Ph) and Pd@PMO(Ph) catalysts. As shown in Table 1, only trace of the target product 1,4-diphenyl-1,3-butadiene was detected in the presence of single Rh@PMO(Ph), though the conversion of cinnamaldehyde reached to 71%. This demonstrated that most of the cinnamaldehyde converted into the 1-phenyl-1,3-butadiene rather than to the target product of 1,4-diphenyl-1,3-butadiene in the absence of Pd@PMO(Ph). Similarly, nearly no reactions occurred (cinnamaldehyde conversion = 5.0%) when the single Pd@PMO(Ph) catalyst was employed. However, when the 1-phenyl-1,3-butadiene was used instead of cinnamaldehyde as the original reactant, 89% conversion and 79% selectivity toward the target product 1,4-diphenyl-1,3-butadiene were obtained over the single Pd@PMO(Ph) catalyst. Those results confirmed that the cinnamaldehyde methylenation was mainly catalyzed by the Rh@PMO(Ph) while the Heck reaction was mainly catalyzed by the Pd@PMO(Ph). Considering the Rh/Pd@PMO(Ph) series catalysts, both the activity and the selectivity first increased and then decreased with the increase of Rh(I) and Pd(II) loading. The optimum Rh(I) and Pd(II) loadings were determined as 1.7 wt% and 0.54 wt%, corresponding to the Rh/Pd@PMO(Ph)-10 catalyst. The poor efficiency obtained at low Rh(I) and Pd(II) loading might be attributed to the long-distance between two neighboring Rh(I) active sites and two neighboring Pd(II) active sites, taking into account that both the cinnamaldehyde methylenation and Heck reaction need two neighboring active sites for the cross-coupling reactions. However, very high Rh(I) and Pd(II) loadings were also harmful for catalytic efficiency, possibly due to the decrease of the ordering degree of mesoporous structure, which might enhance the diffusion limit, the increase of inaccessible active sites, and the change of the chemical microenvironments of Rh(I) and Pd(II) active sites.

Table 1 also summarized the catalytic efficiencies obtained from the Rh/Pd@PMO(Ph)-10 and other catalyst systems. One could see that the Rh/Pd@PMO(Ph)-10 exhibited both higher activity and better selectivity than the Rh/Pd@PPh_2-PMO(Ph)-10 with the similar Rh(I) and Pd(II) loadings. On one hand, the lower activity and selectivity of the Rh/Pd@PPh_2-PMO(Ph)-10 might be due to the pore blockage since the organometal complexes were terminally bonded to the pore surface rather than incorporated into the silica walls in the Rh/Pd@PMO(Ph)-10, leading to the enhanced steric hindrance for the diffusion and adsorption of the reactant molecules. On the other hand, the Rh/Pd@PPh_2-PMO(Ph)-10 displayed a different coordination model from the Rh/Pd@PMO(Ph)-10. In the Rh/Pd@PPh_2-PMO(Ph)-10, each metal ion coordinated with one PPh_3- and one or two $(CH_2CH_2)PPh_2$-ligands. However, in the Rh/Pd@PMO(Ph)-10, each metal ion coordinated with two or three $(CH_2CH_2)PPh_2$-ligands. As mentioned above, the XPS spectra demonstrated that $(CH_2CH_2)PPh_2$-ligand could donate more electrons to Rh(I) and Pd(II) in the corresponding complexes, which would inevitably affect the catalytic performances of the Rh(I) and/or Pd(II) active sites [16]. The Rh/Pd@PMO(Ph)-10 also exhibited much higher activity and selectivity than the combined Rh@PMO(Ph) and Pd@PMO(Ph) catalytic system obtained by mechanical mixture, showing the synergic effect between Rh(I) and Pd(II) active sites, which supplied an indirect evidence for the co-condensation between Rh(I) silane and Pd(II) silane rather than the separate condensation of either Rh(I) silane or Pd(II) silane. Such promoting effect could also be observed by comparing the catalytic efficiency of the Rh/Pd@PMO(Ph)-10 with either the mixed $RhCl(PPh_3)_3$ and Pd@PMO(Ph) or the mixed $PdCl_2(PPh_3)_2$ and Rh@PMO(Ph) system. The Rh/Pd@PMO(Ph)-10 displayed the comparable catalytic efficiency with the homogeneous catalyst system containing mixed $RhCl(PPh_3)_3$ and $PdCl_2(PPh_3)_2$. To make sure whether the Rh(I) and Pd(II) organometals incorporated into the PMO(Ph) support or the homogeneous Rh(I) and Pd(II) organometals leached from the solid catalyst were the real catalysts, the following experiment was carried out according to the standard procedure proposed by Sheldon et al. [46]. Firstly, the reaction was allowed to proceed for 12 h until the cinnamaldehyde conversion exceeded 45%. Then, the reaction mixture was filtered to remove the solid catalyst and the mother liquor was allowed to react for another 24 h under identical conditions. No significant change in either the cinnamaldehyde conversion or the yield to the target

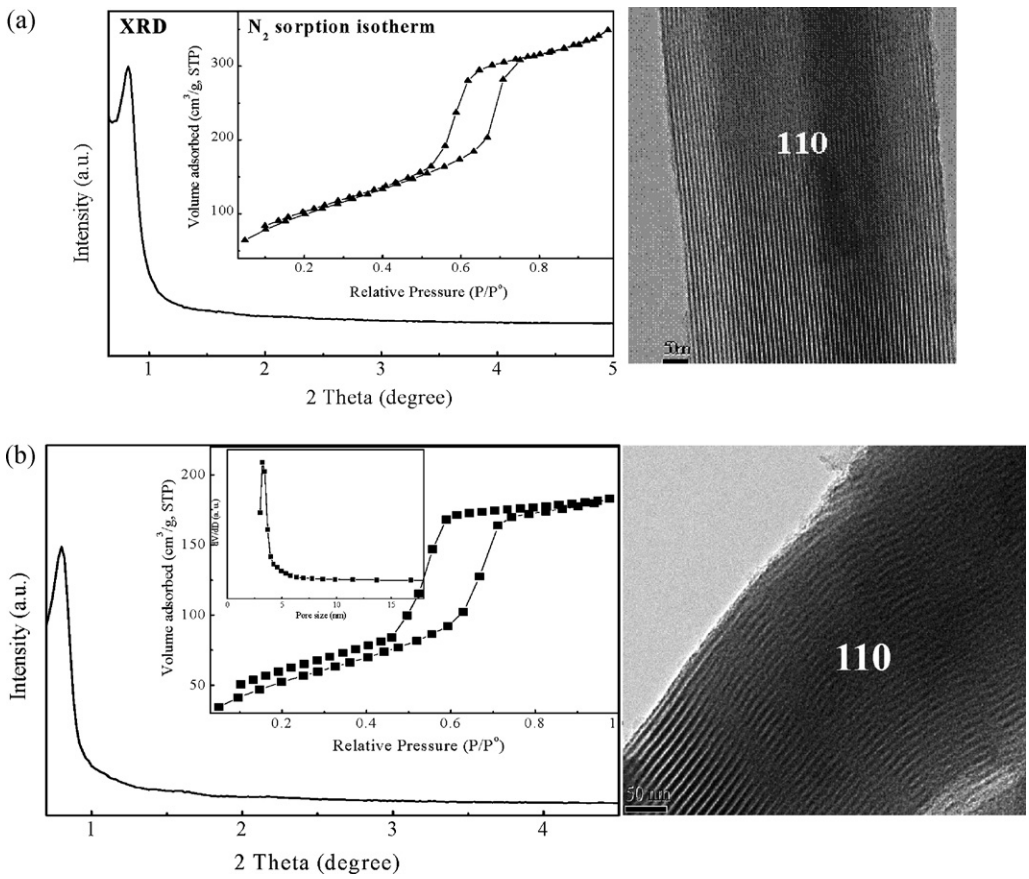

Fig. 7. (a) Low-angle XRD pattern, N_2 adsorption–desorption isotherm, and TEM image of the Cp*Rh@PMO(Et) chiral catalyst and (b) the Rh/Pd@PPh_2-PMO(Ph) catalyst (attached pore size distribution).

Table 1
Structural parameters and catalytic efficiencies of different Rh(I) and Pd(II) series catalysts.[a]

Catalyst	Rh content (mmol)	Pd content (mmol)	S_{BET} (m^2/g)	V_P (cm^3/g)	D_P (nm)	Conv. (%)	Select. (%)
Rh@PMO(Ph)	0.13	–	–	–	–	71	7.0
Pd@PMO(Ph)	–	0.040	–	–	–	5.0	69
Rh/Pd@PMO(Ph)-2.5	0.13	0.064	649	0.51	5.9	66	62
Rh/Pd@PMO(Ph)-5.0	0.13	0.054	650	0.51	5.8	73	64
Rh/Pd@PMO(Ph)-7.5	0.13	0.048	617	0.50	5.8	88	68
Rh/Pd@PMO(Ph)-10	0.13	0.040	595	0.49	5.8	91	71
Rh/Pd@PMO(Ph)-15	0.13	0.053	435	0.36	4.1	92	61
Rh/Pd@PPh_2-PMO(Ph)-10	0.13	0.067	256	0.30	3.1	88	67
Rh@PMO(Ph) + Pd@PMO(Ph)	0.13	0.040	–	–	–	60	60
$RhCl(PPh_3)_3$ + Pd@PMO(Ph)	0.13	0.040	–	–	–	87	69
Rh@PMO(Ph) + $PdCl_2(PPh_3)_2$	0.13	0.040	–	–	–	79	79
$RhCl(PPh_3)_3$ + $PdCl_2(PPh_3)_2$	0.13	0.040	–	–	–	94	82

[a] Reaction conditions: 1.0 mmol cinnamaldehyde, 1.4 mmol trimethylsilyldiazomethane, 1.1 mmol *i*PrOH, 1.1 mmol PPh_3, 1.0 mmol iodobenzene and 5.0 mL THF, T = 60 °C, t = 24 h.

product 1,4-diphenyl-1,3-butadiene was detected, indicating that the present catalysis indeed was heterogeneous in nature.

Similar results were also observed from the Fe/Cp*Rh@PMO(Et) catalyst in the one-pot cascade reaction comprised sequential Fe(III)-catalyzed phenylacetylene hydrolysis and Cp*Rh-catalyzed asymmetric hydrogenation (Eq. (2)). As shown in Table 2, at the optimum Cp*Rh and Fe(III) loadings, the Fe/Cp*Rh@PMO(Et) showed not only the comparable activity but also the equivalent ee value with the corresponding homogeneous catalytic system comprising $FeCl_3$ and $(Cp^*RhCl_2)_2$.

The most important advantage of the immobilized catalysts was that they could be easily recycled and used repetitively. As shown in Fig. 8(a), the Rh/Pd@PMO(Ph)-10 could be used repetitively for 4 times without significant decrease in the yield of the target product 1,4-diphenyl-1,3-butadiene. However, the Rh/Pd@PPh_2-PMO(Ph)-10 obtained by post-grafting displayed a rapid deactivation during the recycling test. ICP analysis demonstrated no significant leach of either the Rh(I) or the Pd(II) species from the Rh/Pd@PMO(Ph)-10 catalyst occurred during 4 cycles of reactions. However, more than 20% Rh(I) and Pd(II) species leached off from the Rh/Pd@PPh_2-PMO(Ph)-10 catalyst were detected after being used repetitively for 3 times, which could sufficiently account for the rapid decrease in the catalytic efficiency. Similarly, the Fe/Cp*Rh@PMO(Et) also displayed strong durability in one-pot cascade reaction containing sequential Fe(III)-catalyzed phenylacetylene hydrolysis and Cp*Rh-catalyzed asymmetric hydrogenation. As shown in Fig. 8(b), the

Table 2
Structural and catalytic properties of $FeCl_3$ and Cp*Rh@PMO(Et) system.[a]

Catalyst	Rh loading (mmol/g)	S_{BET} (m^2/g)	V_P (cm^3/g)	D_P (nm)	Conv. (%)	Select. (%)	Yield (%)	ee (%)
Fe/Cp*Rh@PMO(Et)-2.5	0.034	683	0.78	3.4	92	84	78	94
Fe/Cp*Rh@PMO(Et)-5.0	0.058	565	0.69	3.4	93	86	80	>99
Fe/Cp*Rh@PMO(Et)-7.5	0.10	488	0.58	3.4	97	88	86	>99
Fe/Cp*Rh@PMO(Et)-10	0.12	437	0.53	3.0	90	80	72	93
$FeCl_3$ + $(Cp^*RhCl_2)_2$	–	–	–	–	96	91	88	>99

[a] Reaction conditions: a Cp*Rh@PMO(Et) catalyst containing 0.010 mmol Cp*Rh, 1.0 mmol $FeCl_3$, 1.0 mmol phenylacetylene, 1.5 mmol HCOONa (pH = 8.0–10), 4.0 mL H_2O, T = 40 °C, t = 24 h.

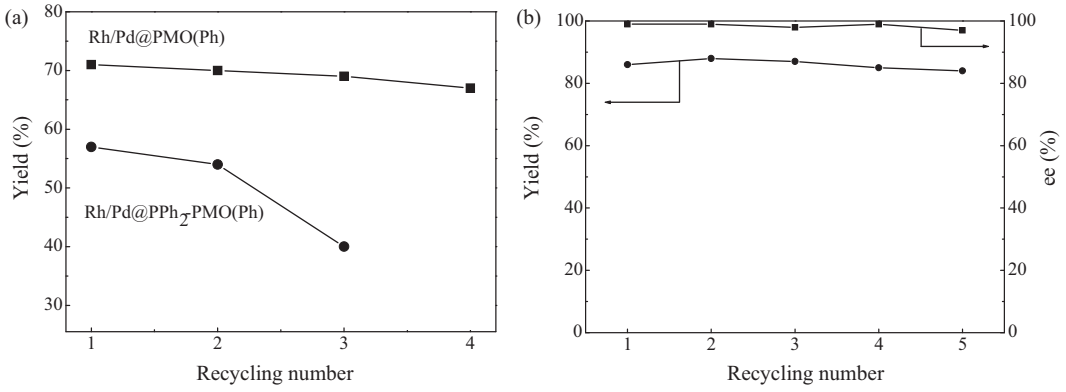

Fig. 8. (a) Recycling test of Rh/Pd@PMO(Ph)-10 and Rh/Pd@PPh_2-PMO(Ph) in the cascade reaction. Reaction conditions: a Rh/Pd@PMO(Ph)-10 catalyst containing 0.13 mmol Rh(I) and 0.040 mmol Pd(II) or a Rh/Pd@PPh_2-PMO(Ph) containing 0.13 mmol Rh(I) and 0.067 mmol Pd(II), 1.0 mmol cinnamaldehyde, 1.4 mmol trimethylsilyldiazomethane, 1.1 mmol *i*PrOH, 1.1 mmol PPh_3, 1.0 mmol iodobenzene and 5.0 mL THF, reaction temperature = 60 °C, reaction time = 24 h. (b) Recycling test of the Fe/Cp*Rh@PMO(Et) catalyst in water-medium "one-pot" cascade reaction. Reaction conditions: a Fe/Cp*Rh@PMO(Et) catalyst containing 0.010 mmol Rh(I), 1.0 mmol $FeCl_3$, 4.0 mL H_2O, 1.5 mmol HCOONa, reaction temperature = 40 °C, reaction time = 24 h.

catalyst could be used repetitively for more than 5 times without significant decrease in either the yield toward target product or the ee value.

4. Conclusions

This work developed a novel approach to synthesize bifunctional catalysts containing two kinds of organometal complexes uniformly incorporated into the silica walls of the periodic mesoporous organosilica (PMO). The as-prepared Rh/Pd@PMO(Ph) and Fe/Cp*Rh@PMO(Et) exhibited comparable activities, selectivities and even ee values in one-pot two-step cascade reactions comprising cinnamaldehyde methylenation and Heck reaction, or phenylacetylene hydrolysis and asymmetric hydrogenation. Meanwhile, they could be easily recycled and used repetitively. Other powerful bifunctional catalysts and even the immobilized enzyme catalysts could also be designed by the present method, which offered more opportunities for the industrial applications.

Acknowledgments

This work is supported by Natural Science Foundation of China (20825724), and Shanghai Government (10dj1400100) (10DJ1400101 and 10PJ1408200).

References

[1] C.T. Kresge, M.E. Leonowicz, W.J. Roth, J.C. Vartuli, J.S. Beck, Nature 359 (1992) 710–712.
[2] J.S. Beck, W.J.C. Vartuli, E.W. Sheppard, S.B. McCullen, J. Am. Chem. Soc. 114 (1992) 10834–10843.
[3] Y. Wan, D.Q. Zhang, N. Hao, D.Y. Zhao, Int. J. Nanotechnol. 4 (2007) 66–69.
[4] A. Vinu, K.Z. Hossain, D. Ariga, J. Nanosci. Nanotechnol. 5 (2005) 347–371.
[5] D.M. Antonelli, J.Y. Ying, Angew. Chem. Int. Ed. 35 (1996) 426–430.
[6] Z.-R. Tian, W. Tong, N.-G. Duan, V.V. Krishnan, S.L. Suib, Science 276 (1997) 926–930.
[7] S. Inagaki, S. Guan, Y. Fukushima, O. Terasaki, J. Am. Chem. Soc. 121 (1999) 9611–9614.
[8] T. Asefa, M.J. Maclachlan, N. Coombs, G.A. Ozin, Nature 402 (1999) 867–871.
[9] K.J. Shea, D.A. Loy, Chem. Mater. 13 (2001) 3306–3319.
[10] F. Hoffmann, M. Cornelius, J.M. Fröba, Angew. Chem. Int. Ed. 45 (2006) 3216–3251.
[11] T. Asefa, M. Kruk, N. Coombs, M. Jaroniec, G.A. Ozin, J. Am. Chem. Soc. 125 (2003) 11662–11673.
[12] W.A. Herrmann, B. Cornils, Angew. Chem. Int. Ed. 36 (1997) 1048–1067.
[13] Y. Hayashi, Angew. Chem. Int. Ed. 45 (2006) 8103–8104.
[14] F.X. Zhu, W. Wang, H.X. Li, J. Am. Chem. Soc. 133 (2011) 11632–11640.
[15] F. Zhang, C.M. Kang, H.X. Li, Adv. Funct. Mater. 21 (2011) 3189–3197.
[16] H.X. Li, H. Yin, F. Zhang, H.X. Li, Y.N. Huo, Y.F. Lu, Environ. Sci. Technol. 43 (2009) 188–194.
[17] J.L. Huang, F.X. Zhu, F. Zhang, W. Wang, H.X. Li, J. Am. Chem. Soc. 132 (2010) 1492–1493.
[18] Y.Q. Sun, G.H. Liu, T.Z. Huang, Y.L. Zhang, H.X. Li, Chem. Commun. 47 (2011) 2583–2585.
[19] F. Zhang, X.S. Yang, F.X. Zhu, J.L. Huang, W. Wang, H.X. Li, Chem. Sci. 3 (2012) 476–484.
[20] L.F. Tietze, G. Brasche, K. Gericke, Domino Reactions in Organic Synthesis, Wiley-VCH, Weinheim, Germany, 2006.
[21] M. Beller, C. Bolm, Transition Metals for Organic Synthesis: Building Blocks and Fine Chemicals, Wiley-VCH, Weinheim, 2004.
[22] B. Breit, S.K. Zhan, Angew. Chem. Int. Ed. 40 (2001) 1910–1913.
[23] D. Enders, C. Grondal, M.R.M. Huttl, Angew. Chem. Int. Ed. 46 (2007) 1570–1581.
[24] T.-L. Ho, Tandem Organic Reactions, Wiley-Interscience, New York, 1992.
[25] N. Hall, Science 266 (1994) 32–34.
[26] J.D. White, J. Hong, L.A. Robarge, Tetrahedron Lett. 40 (1999) 1463–1466.
[27] A.C. Tim, H.L. Tristan, J. Am. Chem. Soc. 131 (2009) 3124–3125.
[28] Q. Yang, J. Liu, J. Yang, S. Inagaki, C. Li, J. Catal. 228 (2004) 265–272.
[29] D.E. De Vos, I.F.J. Vankelecom, P.A. Jabobs, Chiral Catalyst Immobilization and Recycling, Wiley-VCH, Weinheim, 2000.
[30] C. Li, Catal. Rev. 46 (2004) 419–492.
[31] Y. Wan, J. Chen, D.Q. Zhang, H.X. Li, J. Mol. Catal. 258 (2006) 89–94.
[32] H. Huang, R. Yang, D. Chinn, C. Munson, J. Ind. Eng. Chem. Res. 42 (2003) 2427–2433.
[33] H.X. Li, F. Zhang, Y.F. Lu, Green Chem. 9 (2007) 500–505.
[34] D.M. Jiang, J.S. Gao, Q.H. Yang, J. Yang, C. Li, Chem. Mater. 18 (2006) 6012–6018.
[35] S. Inagaki, S. Guan, O. Terasaki, Nature 416 (2002) 304–307.
[36] P.F.W. Simon, R. Ulrich, H.W. Spiess, U. Wiesner, Chem. Mater. 13 (2001) 3464–3486.
[37] O. Kühl, Phosphorus-31 NMR Spectroscopy, Springer-Verlag, Berlin, Heidelberg, 2008.

[38] D.Y. Zhao, Q.S. Huo, B.F. Chmelka, G.D. Stucky, J. Am. Chem. Soc. 120 (1998) 6024–6036.
[39] H.H. Wagner, H. Hausmann, W.F. Holderich, J. Catal. 203 (2001) 150–156.
[40] F. John, F.W. Moulder, J. Chastain, Handbook of X-ray Photoelectron Spectroscopy, Perkin-Elmer Corporation Physical Electronics Division, 1992.
[41] A.P.H.J. Schenning, F. Biscarini, S.C.J. Meskers, J. Am. Chem. Soc. 124 (2002) 1269–1275.
[42] W.C. Li, A. Lu, C. Weidenthaler, F. Schüth, Chem. Mater. 16 (2004) 5676–5681.
[43] J.R. Matos, M. Kruk, G.A. Ozin, T. Kamiyama, J. Terasaki, Chem. Mater. 14 (2002) 1903–1905.
[44] R. Xing, N. Liu, Y.W. Jiang, L. Chen, M.Y. He, P. Wu, Adv. Funct. Mater. 17 (2007) 2455–2461.
[45] A. Corma, D. Das, H. Garcia, A. Leyva, J. Catal. 229 (2005) 322–331.
[46] R.A. Sheldon, M.I. Wallau, W.C.E. Arends, U. Schuchardt, Acc. Chem. Res. 31 (1998) 485–493.